Reactions with the double-Borromean nucleus ^{8}He

A. Lemasson,[1] A. Navin,[1,*] N. Keeley,[2] M. Rejmund,[1] S. Bhattacharyya,[1,3] A. Shrivastava,[4] D. Bazin,[5] D. Beaumel,[6] Y. Blumenfeld,[6] A. Chatterjee,[4] D. Gupta,[6,†] G. de France,[1] B. Jacquot,[1] M. Labiche,[7] R. Lemmon,[7] V. Nanal,[8] J. Nyberg,[9] R. G. Pillay,[8] R. Raabe,[1,‡] K. Ramachandran,[4] J. A. Scarpaci,[6] C. Simenel,[10] I. Stefan,[1,§] and C. N. Timis[11]

[1]*GANIL, CEA/DSM-CNRS/IN2P3, Bd Henri Becquerel, BP 55027, F-14076 Caen Cedex 5, France*

[2]*Department of Nuclear Reactions, The Andrzej Sołtan Institute for Nuclear Studies, ul. Hoża 69, PL-00681 Warsaw, Poland*

[3]*Variable Energy Cyclotron Centre, 1/AF Bidhan Nagar, Kolkata 700064, India*

[4]*Nuclear Physics Division, Bhabha Atomic Research Centre, Mumbai 400085, India*

[5]*National Superconducting Cyclotron Laboratory, Michigan State University, East Lansing, Michigan, 48824, USA*

[6]*Institut de Physique Nucléaire, IN2P3-CNRS, 91406 Orsay, France*

[7]*CRLC, Daresbury Laboratory, Daresbury, Warrington WA4 4AD, United Kingdom*

[8]*Department of Nuclear and Atomic Physics, Tata Institute of Fundamental Research, Mumbai 400005, India*

[9]*Department of Physics and Astronomy, Uppsala University, Uppsala, Sweden*

[10]*IRFU/Service de Physique Nucléaire, CEA Centre de Saclay, F-91191 Gif-sur-Yvette, France*

[11]*Department of Physics, University of Surrey, Guildford GU2 7XH, United Kingdom*

(Received 15 September 2010; published 29 October 2010)

Differential cross sections for elastic-scattering and neutron-transfer reactions along with cross sections for fusion in the ^{8}He+^{65}Cu system are reported at energies above the Coulomb barrier ($E_{\rm lab}$ = 19.9 and 30.6 MeV). The present work demonstrates the feasibility of using inclusive measurements of characteristic in-beam γ rays with low-intensity ($\sim 10^{5}$ pps) radioactive ion beams to obtain the residue cross sections for fusion and neutron transfer. Exclusive measurements of γ rays in coincidence with light charged particles have been used to further characterize the direct reactions induced by this double-Borromean nucleus. Coupled reaction channels calculations are used to illustrate the important role played by the transfer channels and to help in understanding the influence of the structure of ^{8}He on the reaction mechanism.

DOI: 10.1103/PhysRevC.82.044617 PACS number(s): 25.60.−t, 25.70.Hi, 25.70.Jj

I. INTRODUCTION

The advent of reaccelerated beams using Isotope Separation On Line (ISOL) techniques provides new opportunities to study and understand reactions with nuclei far from stability [1–4]. The neutron separation energies of neutron-rich nuclei near the drip line are considerably smaller ($S_n \sim 1$ MeV) than those for typical stable nuclei ($S_n \sim 8$ MeV). In addition to the large spatial extent (halo) of the weakly bound valence nucleon(s), these nuclei can also exhibit Borromean structure [5] (three-body bound systems in which none of the two-body subsystems are bound). Typical examples include ^{6,8}He, ^{11}Li, and, more recently, ^{22}C [6], which can be viewed as three-body systems consisting of a core nucleus and two valence neutrons. These properties are expected to influence the reaction processes and are also relevant to reactions of astrophysical interest [7]. The large probability of breakup associated with the weak binding of the valence nucleon(s) led to the expectation that breakup of the projectile would be a dominant channel and also influence the reaction mechanism for these nuclei [1,2,4]. In particular, the influence of breakup on fusion reactions around the barrier has been of considerable interest [1,8]. Attempts have been made to understand the influence of the breakup process on the fusion and elastic scattering of beams of both stable and radioactive weakly bound nuclei using various approaches [9–13]. However, the loosely bound valence nucleon(s) could also imply large transfer cross sections from the projectile to the target. This in turn would also be expected to influence the reaction mechanism. Large transfer cross sections have been reported for ^{6}He beams on ^{65}Cu [14,15], ^{64}Zn [16], ^{197}Au [17], ^{209}Bi [18,19], and ^{238}U targets [20,21]. References [14,19] also showed that the transfer cross sections were even larger than those for breakup. More recently, large transfer cross sections ($1n + 2n$) were also reported in the ^{8}He+^{197}Au system at energies below and above the Coulomb barrier [22]. The effect of transfer on other channels was theoretically investigated using coupled reaction channels (CRC) calculations [4]. In order to have a complete understanding of the reaction mechanisms for neutron-rich nuclei, measurements of all the reaction channels are necessary.

Experimental investigations involving low-energy (around the Coulomb barrier) and low-intensity radioactive ion beams (RIB) have brought about new challenges. In general, investigations with low-intensity radioactive ion beams ($\sim 10^{5}$ pps) have been restricted due to both the limited availability of ISOL beams and the need for a substantial increase in experimental sensitivity given the typical reduction by a factor of $\sim 10^{6}$ in intensity compared to stable beams. The direct measurement

*navin@ganil.fr

†Permanent address: Dept. of Physics and Centre for Astroparticle Physics and Space Science, Bose Institute, Kolkata 700091, India.

‡Permanent address: Instituut voor Kern- en Stralingsfysica, K.U. Leuven, Celestijnenlaan 200D, B-3001 Leuven, Belgium.

§Permanent address: Institut de Physique Nucléaire, IN2P3-CNRS, 91406 Orsay, France.

of residues produced in reactions induced by light projectiles at these energies is difficult given their low recoil velocities. Measurements of reaction products using the in-beam γ-ray technique are much more challenging compared to stable beams due to the relatively lower yields and the additional background arising from the radioactive decay of the beam particles. The first inclusive γ-spectroscopy measurement using a 10^9-pps reaccelerated RIB was performed by Catford *et al.* [27] using a beam of ^{19}Ne. More recently absolute cross-section measurements (both inclusive and exclusive) in the ^{6}He+^{65}Cu system with intensities of $\sim 10^7$ pps have been reported [14,15]. Inclusive measurements may not be able to separate various processes like fusion and direct reactions which could lead to similar final states. This is particularly true for reactions induced by light neutron-rich nuclei on medium mass targets [14–16]. Studies of transfer reactions with Borromean nuclei on medium and heavy targets necessitate exclusive measurements. Particle (both charged and neutral) γ coincidences [14] or particle correlations [9] have been shown to be a powerful tool to characterize the various reaction processes using ^{6}He RIB. More recently new limits of sensitivity enabling accurate and precise cross sections to be obtained using off-beam measurements with beam intensities of $\sim 10^5$ pps have also been reported [22].

With a half-life $t_{1/2} = 119.1$ ms, ^{8}He is the most neutron-rich bound nucleus known today and is an ideal candidate to study the influence of nuclear structure on the reaction mechanism around the Coulomb barrier. Accurate measurements of its charge radius [28] and mass [29] were recently reported. A significant reduction in charge radius from ^{6}He to ^{8}He was interpreted as a change in the correlations of the valence neutrons. The helium isotopic chain is an ideal laboratory to study the effect of the dramatic variation of the intrinsic properties on the reaction mechanism. Figure 1(a) shows the low-lying energy levels of the helium isotopes. The neutron emission threshold has the largest variation for a single isotopic chain, from 20.5 MeV for the tightly bound ^{4}He to 0.9 MeV for ^{6}He [see Fig. 1(b)]. Additionally, this is the only isotopic chain where the two-neutron separation energy S_{2n} increases as the neutron drip line is approached. The structure of ^{8}He has been investigated using the direct reactions ^{8}He$(p, d)^7$He [30] and ^{8}He$(p, t)^6$He [31], quasi-free scattering [32], and knock-out reactions [33,34]. The low-lying spectrum of ^{8}He was also recently studied by means of the ^{3}H(^{6}He,p)^{8}He reaction [35]. The ground-state configuration of ^{8}He (involving $\nu^4_{3/2}$ [36] or $\nu^2_{3/2}\nu^2_{1/2}$ [31,32,37]) is still an open question. The ground state of ^{8}He can be considered to be composed of a ^{4}He+4n or ^{6}He+2n structure. The possibility of a significant contribution from the ^{6}He (2^+) first excited state to the ^{8}He ground state has also been investigated [31,38]. As ^{6}He is a Borromean nucleus, ^{8}He could be considered to be a "double-Borromean" nucleus. The study of transfer reactions induced by neutron-rich nuclei like ^{8}He, associated with predictions of possible dineutron correlations [37,39], could be used as a tool to probe pairing in finite fermionic systems [40,41].

The motivation of this work is to measure for the first time elastic-scattering, transfer, and fusion cross sections for ^{8}He at energies around the Coulomb barrier and understand

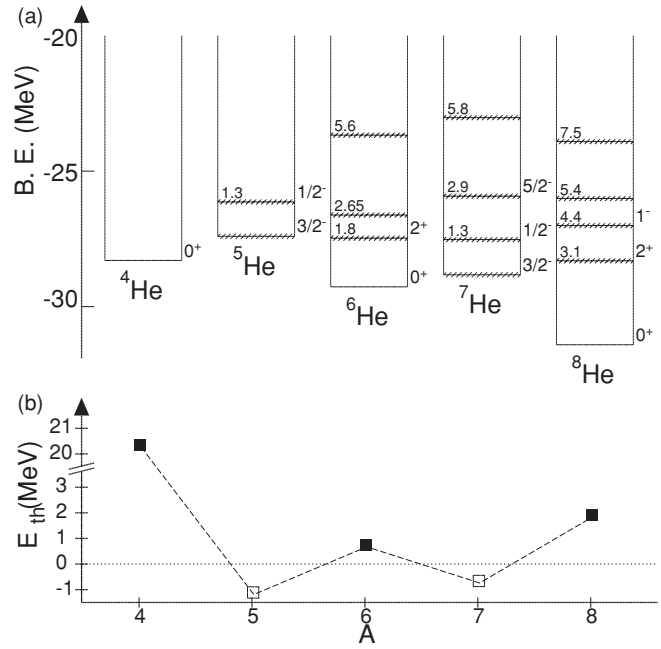

FIG. 1. (a) Low-lying states in $^{4-8}$He isotopes (Refs. [23–26]). (b) Lowest particle emission thresholds in the helium isotopic chain. Full (open) symbols represent the bound (unbound) isotopes. The line is to guide the eye.

the effect of its intrinsic properties, described above, on the reaction dynamics. Simultaneously, the goal is to improve the sensitivity of in-beam measurements with low-intensity ISOL beams. Inclusive measurements of prompt γ rays were used to obtain the heavy residue cross sections (fusion and neutron transfer), while exclusive coincidence measurements between γ rays and light charged particles were used to obtain the individual contributions arising from neutron transfer and breakup mechanisms. The measured angular distributions and total cross sections are discussed within the framework of coupled reaction channels calculations. In the next section, the experimental details are presented. This is followed by a detailed analysis, discussion, and summary of the work.

II. EXPERIMENTAL SETUP AND ANALYSIS

Beams of radioactive ^{8}He ions were obtained from the SPIRAL ISOL facility at Grand Accelerateur National D'Ions Lourds (GANIL) [3,42]. The fragmentation of a 75-MeV/nucleon ^{13}C beam on a thick graphite target was used to produce the ^{8}He ions which were reaccelerated by the CIME cyclotron to 19.9 and 30.6 MeV. The ^{8}He beams, with an energy resolution $\frac{\Delta E}{E} \sim 10^{-3}$, a beam spot size of less than 5 mm (FWHM), and an average intensity of 2×10^5 pps, were incident on a 2.68-mg/cm^2-thick self-supporting ^{65}Cu foil (isotopically enriched to 99.7%). The intensity of the ^{8}He beam particles was measured using a plastic scintillator 2 in. in diameter (placed 7 m after the target, the beam was refocused using a pair of quadrupoles). A microchannel plate (MCP) detector, placed on a movable arm 2 m upstream of the target position, was also used to monitor the beam. A schematic

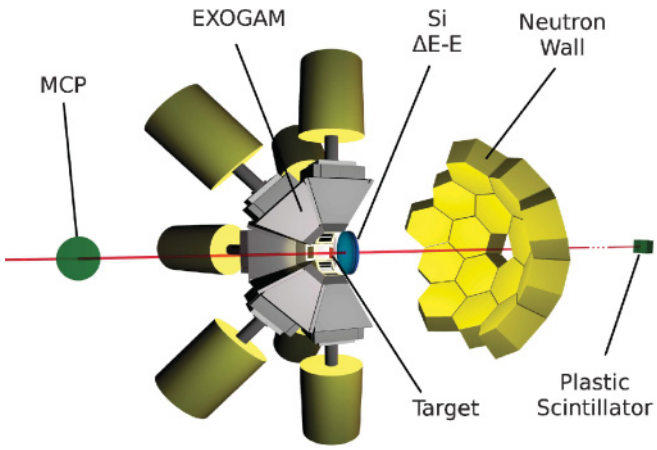

FIG. 2. (Color online) Schematic of the experimental setup showing the EXOGAM γ array, the silicon ΔE-E annular telescope, and the Neutron Wall. The beam-monitoring detectors [Micro-Channel Plate (MCP) and plastic scintillator] are also shown.

of the experimental setup is shown in Fig. 2. Characteristic γ rays from targetlike residues produced in the reaction were detected using the EXOGAM γ array [43] consisting of 11 fully Compton-suppressed clovers placed 14.7 cm from the target. The individual clovers were operated in add-back mode. The photo-peak efficiency of the array was ~6.1% and typical energy resolution was ~2.4 keV at $E_\gamma = 1332$ keV. The charged particles were detected and identified in an annular Si telescope, placed at 2.5 cm from the target, comprising ΔE (~50 μm) and E (~500 μm) elements with active inner and outer diameters of 22 and 70 mm covering an angular range of 25°–60° (16 rings and 96 sectors). The angular resolution was ~1.7°. The energy resolution for elastically scattered particles was ~300 keV. Monte Carlo simulations, taking into account the size of the beam and the geometry of the ΔE-E detector, were used to obtain the center-of-mass angle and solid angle corresponding to each ring and sector. The effects of energy and angular straggling in the target were also taken into account in the simulation. The results of the simulation were verified through elastic-scattering measurements on a ^{197}Au (150 μg/cm^2) target. In addition, neutrons were detected in the Neutron Wall array [44] consisting of 45 hexagonal detectors placed at 55 cm from the target, covering ≈18% of 4π. Inclusive measurements as well as coincidences with charged particles (^{4,6,8}He), neutrons and γ rays were used to unambiguously identify the characteristic γ rays emitted by the targetlike residues.

A. Measurement of targetlike residue cross sections from inclusive γ rays for fusion and neutron transfer

An inclusive γ-ray spectrum obtained at $E_{\rm lab} = 30.6$ MeV is shown in Fig. 3(a). The inclusive γ-ray spectrum is dominated by lines at 1460.82 keV (room background, ^{40}K) and 980.8 keV (emitted in the β decay of ^{8}He). It should be noted that the reduction of the radioactive beam induced background to a level lower than room background represents a significant achievement. In contrast, Fig. 3(b) shows the inclusive γ-ray spectrum obtained under the same conditions but with the MCP detector assembly inserted in the beam. This illustrates the dramatic effect of the implantation of radioactive beam particles around the target position, in this case due to a very small beam halo arising from straggling in the mylar foil of the MCP. The figure shows the spectrum to be completely dominated by the 981-keV γ transition (and the associated 477-keV transition) emitted in the decay of implanted ^{8}He beam particles. This highlights the difficulties that can be expected in performing γ-ray measurements with low-energy radioactive ion beams. Similar issues will arise with other radioactive beams or their daughter nuclei that have a relatively long half-life. The beam was stripped after acceleration through the CIME cyclotron to minimize charge-exchange reactions in the beam transport section and reduce the amount of ^{8}He^{1+} ions which, due to their higher rigidity, ended being implanted near the target. Optimal beam tuning and stopping the beam far away from the target in addition to using narrow and optimal time gates for data collection also played an important role. As can be seen in the inset of Fig. 3(a), despite the dominant contribution from unrelated γ transitions, the efficient shielding provided by the anti-Compton BGO shields and the other factors, discussed above, made inclusive measurement of the main evaporation residues possible. With such a low-intensity beam the expected yields for the relevant transitions can be smaller or comparable to the room background.

The measurement of smaller cross sections for the reaction products requires further improvement in the experimental sensitivity. This was achieved using a "prompt" time condition (as mentioned earlier) between the OR of the time-aligned constant fraction discriminators from the various crystals of the EXOGAM γ array and the cyclotron radio-frequency. However, as shown in Fig. 3(d) (top panel), the inclusive time spectrum between the γ rays and the cyclotron radiofrequency is dominated by random events due to the relatively small yields from the reaction. The position and width of the prompt events of the time distribution were obtained by using a coincidence with either charged particles, γ-γ coincidences, or neutrons [see the bottom panel of Fig. 3(d)]. The background subtracted inclusive γ-ray spectrum obtained using the prompt time condition [indicated by the arrow between the dotted lines in Fig. 3(d)] is shown in Fig. 3(c) at $E_{\rm lab} = 19.9$ MeV. Suitable corrections were made to account for the time response for lower-energy transitions due to the narrow time gate. The characteristic γ rays for the various residues can be clearly identified. A comparison with a similar in-beam measurement in the ^{8}He+^{208}Pb system (Fig. 1 of Ref. [45]) better illustrates the advances made. In the absence of other charged particle detectors close to the target (Fig. 2) the use of an MCP detector would have been sufficient to obtain high-quality time-gated γ-ray spectra. The straggling of the beam in the foil of the MCP detector causes a large deterioration of the quality of the charged-particle spectra (mainly at forward angles), thus preventing the simultaneous measurement of angular distribution of direct reactions.

The individual residue cross sections for the ^{8}He+^{65}Cu system were obtained using the corresponding intensities of the well-known, low-lying γ transitions from the measured inclusive γ-ray spectra [14,46]. The presence of an isomeric first excited level ($t_{1/2} = 13.8$ h) in the ^{69}Zn ($p3n$) evaporation

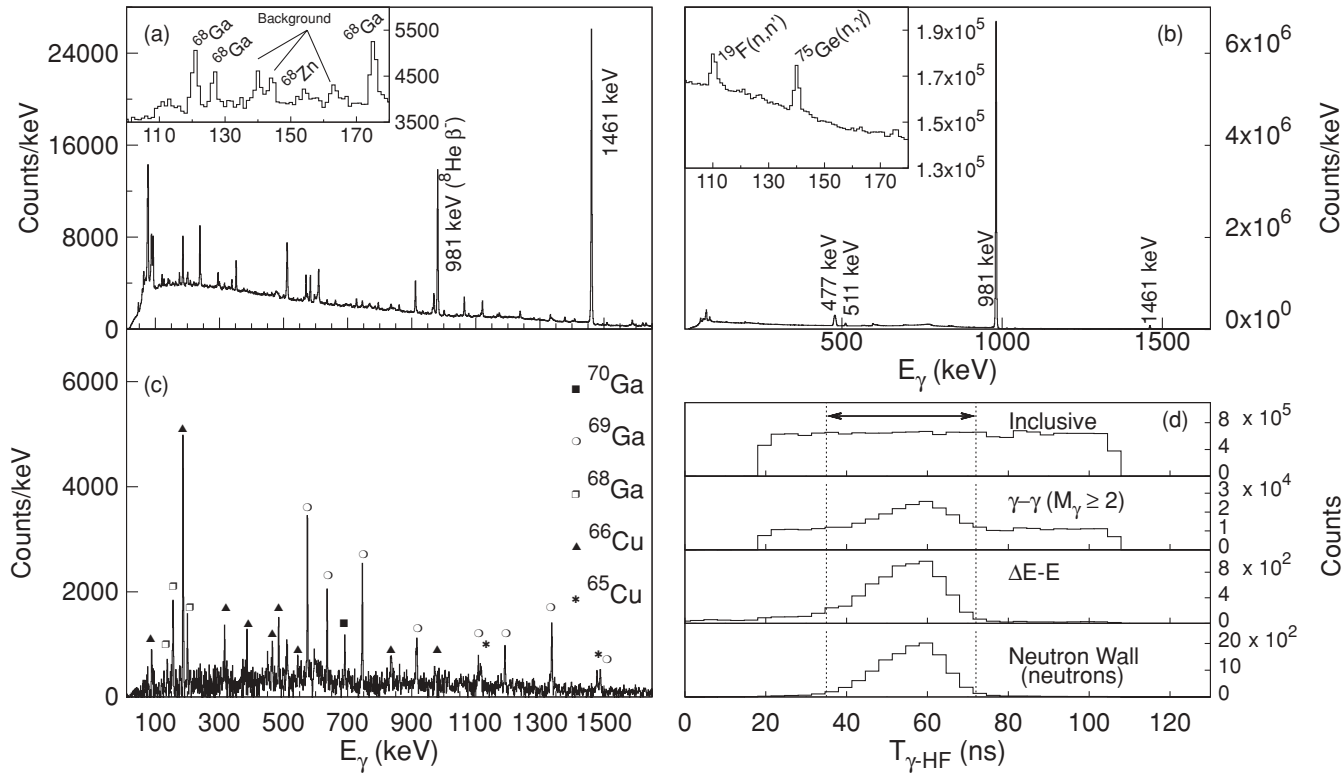

FIG. 3. (a) Inclusive γ-ray spectrum at $E_{\rm lab} = 30.6$ MeV for the ^{8}He+^{65}Cu system. The dominant γ rays arising from room background (1461 keV) and the β decay of ^{8}He (981 keV) are labeled. The inset shows an expansion of the low-energy region where characteristic transitions in ^{69}Ga can be identified. (b) Same as in (a) but with the MCP detector assembly inserted in the beam line (see text). (c) Background subtracted γ spectrum at 19.9 MeV, gated by the time condition between the cyclotron radiofrequency and the OR of the γ-ray detectors for the inclusive spectra shown in the panels of (d). The γ rays arising from fusion evaporation residues and neutron transfer can be clearly seen and are labeled. (d) The different panels show (from top to bottom) the time spectrum between the cyclotron radiofrequency and the OR of the γ-ray detectors inclusive, demanding a γ-γ coincidence in the EXOGAM array in the coincidence with a particle identified in ΔE-E telescope and neutrons in the Neutron Wall. The arrow illustrates the width and the position of prompt condition used.

residues prevented the determination of the cross section for this channel. Corrections due to direct population of the ground states are expected to be small due to the low spins of the nearby levels and have not been made. Figure 4(a) shows the residue cross sections as a function of the center-of-mass energy for the ^{8}He+^{65}Cu system. The lines in the figure are the results of statistical model calculations for the evaporation residues formed in the decay of ^{73}Ga using the statistical model code CASCADE [47]. The level-density formalism of Ignatyuk *et al.* [48] was used, with a level-density parameter $a = A/9$. The transmission coefficients were taken from Refs. [49–51] for the neutron, proton, and α particles, respectively. The angular momentum distribution was obtained from CCFUS [52] using the Akyüz-Winther global parametrization for the nuclear potential [53]. Similar calculations were used to reproduce earlier measurements [14,22]. As can be seen from the figure, the various partial cross sections are reasonably well explained by the statistical model except for the $\alpha 3n$ and $\alpha 4n$ evaporation channels (^{66}Cu and ^{65}Cu residues, respectively). Such a discrepancy between the measured and calculated cross sections for ^{66,65}Cu was observed earlier in the case of ^{6}He+^{65}Cu [14], and was shown to arise from neutron(s)-transfer processes. This is discussed in further detail in the next section. The total fusion cross sections were then obtained from the sum of the individual evaporation cross sections for ^{68,69,70}Ga and ^{68}Zn and corrected for the ^{65,66}Cu and ^{69}Zn contributions using the CASCADE statistical model calculation. These contributions amounted to 36 and 26% at 30.6 and 19.9 MeV, respectively. The errors in the cross sections arising from the uncertainties in measurements of the beam current, γ-ray efficiency, target thickness, available spectroscopic information of the residues, and corrections from the statistical model were estimated to be between 10 and 15%. The integral neutron-transfer cross sections were obtained from the measured intensities of the inclusive γ-ray spectra of ^{65,66}Cu after correcting for compound nucleus contributions calculated using the code CASCADE [47]. The transfer cross sections for the ^{8}He+^{65}Cu system at 19.9 and 30.6 MeV were 782 ± 78 mb and 759 ± 114 mb, respectively, and are shown in Fig. 4(b) along with the fusion cross sections. Additional uncertainty in the total transfer cross sections arising from uncertainties in the statistical model calculations were estimated to be less than 5%. The measured $1n$ and $2n$ transfer cross sections were not corrected for direct population of ground states of ^{66,67}Cu and thus represent lower limits. However, by analogy with the results for the ^{65}Cu$(d,p)^{66}$Cu

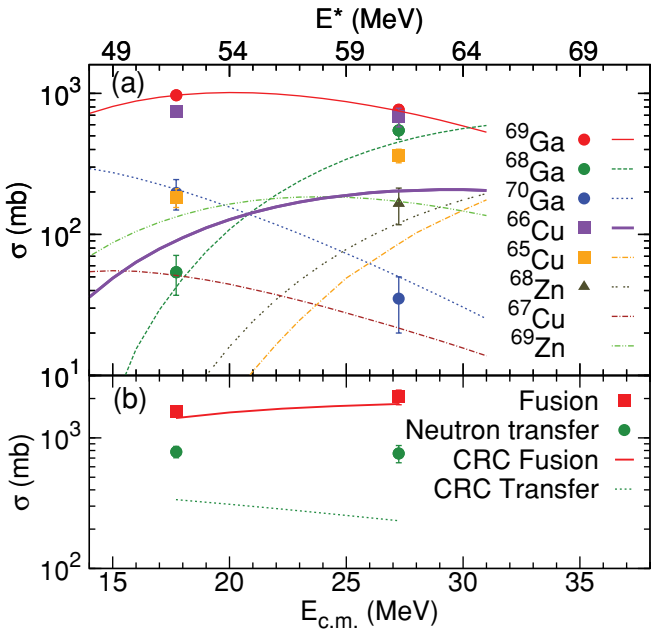

FIG. 4. (Color online) Heavy residue, fusion, and neutron-transfer excitation functions: (a) Measured partial residue cross sections as a function of the center-of-mass energy for the ^{8}He+^{65}Cu system. The lines are obtained using the statistical model code CASCADE (see text). The calculations are normalized to the measured fusion cross sections. (b) Fusion and neutron-transfer cross sections for the ^{8}He+^{65}Cu system. Predictions from coupled reaction channels calculations for fusion (continuous lines) and neutron transfer (dashed lines) are also shown (see text). Only statistical errors are shown.

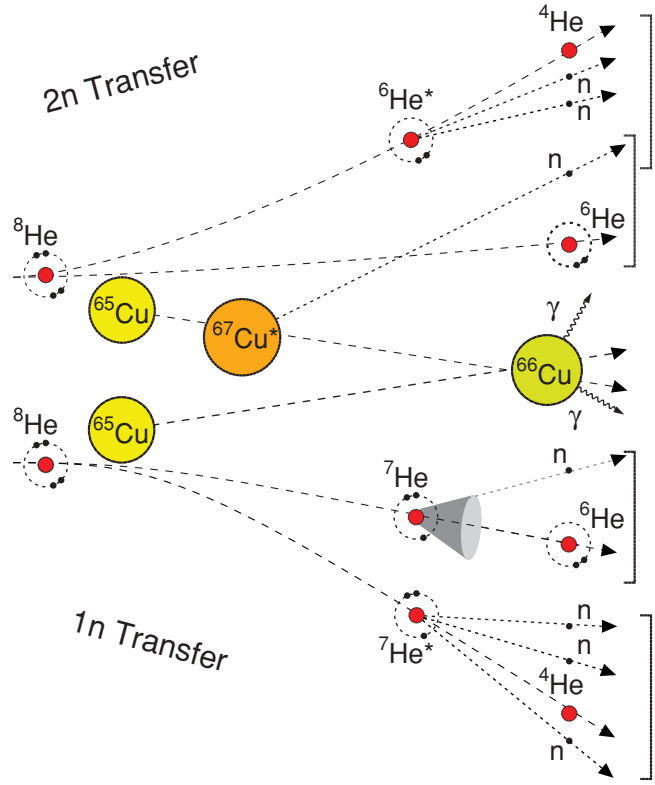

FIG. 5. (Color online) Schematic for $1n$ and $2n$ transfer for ^{8}He+^{65}Cu system illustrating the similar final states formed in a $1n$ and $2n$ transfer reaction involving a Borromean nucleus.

reaction [54], which has a similar Q value to the (^{6}He,^{5}He) and (^{8}He,^{7}He) reactions, direct population of the ground state of ^{66}Cu by $1n$ stripping is expected to be small. This expectation is further supported by the CRC calculations presented in Sec. III, the calculated cross section for direct population of the ^{66}Cu ground state being approximately 2% of the total $1n$-stripping cross section. Direct population of the ^{67}Cu ground state via 2n stripping is effectively ruled out by the very large Q-value mismatch for this reaction.

B. Direct reactions from particle-γ correlations

As opposed to transfer reactions with light ions [55], measurements involving heavy ions are severely restricted by the energy resolution, so normally distributions rather than the populations of discrete states are measured. The large positive Q values for the transfer of neutrons from neutron-rich RIB like ^{8}He to heavy target nuclei additionally amplifies the importance of neutron evaporation following transfer. Particle-γ correlations are a powerful probe for the understanding of such processes and the reaction mechanism in general. The large positive Q values for one- and two-neutron transfer in the ^{8}He+^{65}Cu system ($Q = 4.48$ and 14.04 MeV, respectively) and the semiclassical Q-value matching conditions for neutron transfer (expected to peak near $Q = Q_{\rm opt} = 0$ [56]) favor the population of excited states in such reactions. Thus, excited states in the heavy targetlike residues are populated after a neutron-transfer process. However, the very large Q value for $2n$ transfer suggests that states much above the neutron separation energy in ^{67}Cu ($S_n = 9.1$ MeV) are populated, followed by neutron evaporation to ^{65,66}Cu. In this section particle-γ correlations have been used to obtain a deeper understanding of the transfer angular distributions, with an emphasis on the double-Borromean nature of ^{8}He. Figure 5 illustrates the various final states after a one- and two-neutron transfer in the given system. Additionally, the breakup of the projectile was also investigated. Figure 1(a) shows that both ^{5}He and ^{7}He as well as the excited states of ^{6}He are unbound. ^{5}He and the excited states of ^{6,7}He decay by neutron emission to ^{4}He. Coincidences between ^{6}He and γ rays from ^{65,66}Cu are therefore used to extract the transfer of neutron(s) to the ^{6,7}He ground states, while coincidences between ^{4}He and γ rays from ^{65,66}Cu are used to study neutron transfer to ^{6,7}He excited states. Contributions to ^{4}He-γ coincidences arising from the residues formed after αxn evaporation in a compound nuclear process are accounted for using a statistical model calculation. The summed ($1n + 2n$) neutron-transfer angular distributions were obtained from the exclusive measurements of ^{6}He and ^{4}He in coincidence with characteristic γ rays from ^{65,66}Cu, as described below.

The observed coincidences between ^{6}He and γ transitions in ^{65,66}Cu arise from both $1n$ and $2n$ transfer to the ground states of ^{7}He and ^{6}He, respectively. The Q-value spectrum displayed in Fig. 6(c) illustrates the excitation energy in the targetlike residue. In principle, contributions from $1n$ transfer can also arise from higher-lying resonance states in

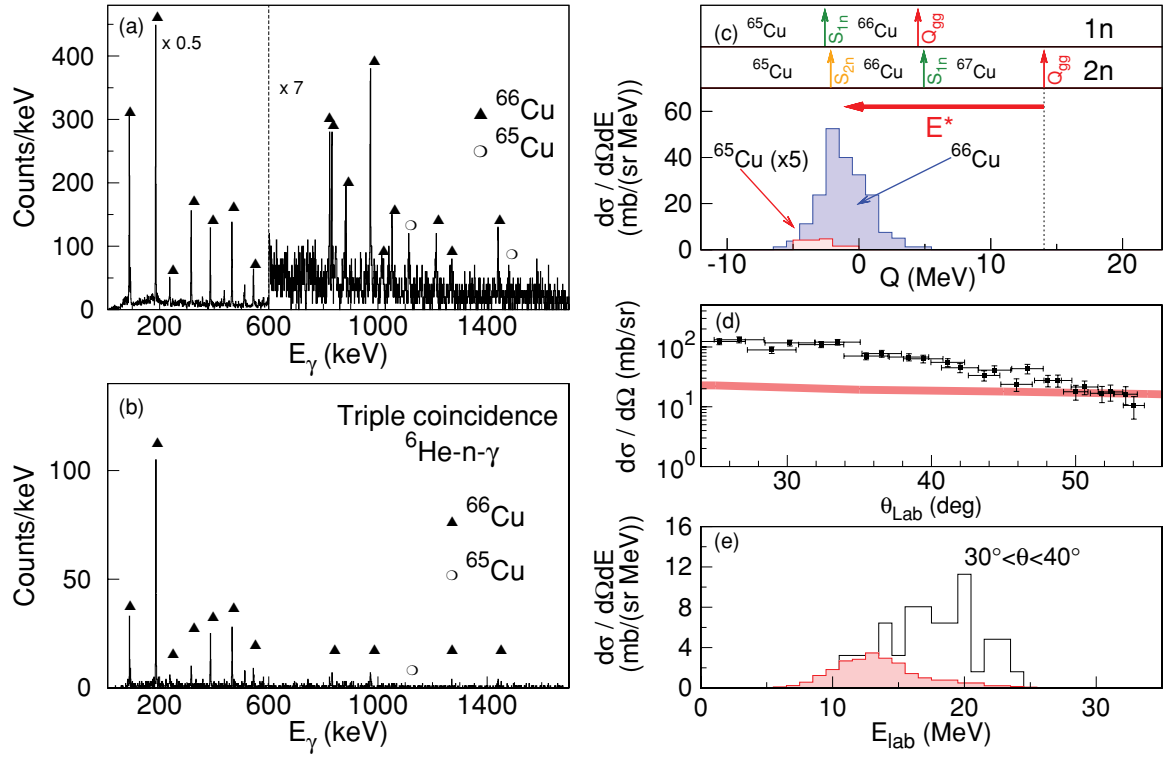

FIG. 6. (Color online) Particle-γ correlations for ^{6}He and ^{4}He (a) γ-ray spectrum in coincidence with ^{6}He particles detected in the telescope at $E_{\rm lab} = 19.9$ MeV. The transitions arising from ^{66,65}Cu are labeled. (b) A triple coincidence spectrum of γ rays requiring detection of a ^{6}He and a neutron. (c) A Q-value distribution for ^{6}He particles, between 30° and 40°, detected in coincidence with either a 185.9-keV γ transition (^{66}Cu) or a 1115.5-keV γ transition (^{65}Cu) at $E_{\rm lab} = 19.9$ MeV. The ground state Q values (Q_{gg}) and separation energies for the transfer of one and two neutrons are labeled. The arrow denotes the excitation energy (E^*) in ^{67}Cu populated in a two-neutron transfer. (d) ^{4}He angular distribution at $E_{\rm lab} = 19.9$ MeV obtained in coincidence with ^{65,66}Cu γ rays. The shaded curve denotes the calculated (using a statistical model) compound nucleus contribution normalized to the measured fusion cross section (the thickness of the line denotes the uncertainty). (e) Energy distribution of α particles detected between 30° and 40° in coincidence with ^{66}Cu γ rays at $E_{\rm lab} = 30.6$ MeV (open histogram) and the calculations for the corresponding $\alpha 3n$ channel (^{66}Cu) from compound nuclear evaporation (filled histogram).

^{7}He, but as the known states are above the ^{6}He $(2^{+})+n$ or ^{4}He$+3n$ thresholds, their contributions to the ^{6}He yield are expected to be small. Figure 6(a) shows a typical γ-ray spectrum in coincidence with ^{6}He and Fig. 6(c) shows the corresponding ^{6}He energy distributions in coincidence with either the 185.9-keV γ transition in ^{66}Cu or the 1115.5-keV γ transition in ^{65}Cu at $E_{\rm lab} = 30.6$ MeV. The nonobservation of ^{67}Cu γ transitions [Fig. 6(a)] and the Q-value spectrum [Fig. 6(c)] of ^{6}He is consistent with the hypothesis of $2n$ transfer followed by evaporation of neutron(s). In the present work, the upper limit on the cross section for the production of ^{67}Cu in a two-neutron-transfer reaction was estimated, using ^{6}He-γ coincidences, to be ∼0.5 and 1.9 mb at 19.9 and 30.6 MeV (as mentioned earlier, these do not represent the $2n$-transfer cross sections). The estimated cross sections are small compared to the measured total transfer cross section reported previously and hence are not considered. ^{6}He angular distributions obtained in coincidence with ^{65,66}Cu γ transition are presented in Figs. 7(a) and 7(b) at $E_{\rm lab} = 19.9$ and 30.6 MeV, respectively. The yields have been corrected for detection efficiency and relative branching of the gating γ-ray transition. The contributions of ^{6}He in coincidence with ^{65}Cu γ rays amount to ∼15% and ∼35% of the total exclusive ^{6}He measurement at 19.9 and 30.6 MeV, respectively. This difference in percentage of the population of ^{65}Cu at the two energies is similar to that observed with ^{6}He and needs to be further understood. This is presumably due to the "kinematic" effects, i.e., Q value and angular momentum matching. This will give rise to a variation with incident energy of the transfer reaction cross sections which will be different for $1n$ and $2n$ transfer.

The situation with ^{4}He-γ coincidences is less straightforward as different mechanisms can contribute to α particle production: (i) the α-xn channel from the decay of the compound nucleus ^{73}Ga (ii) $2n$ transfer to ^{6}He unbound excited states, (iii) $1n$ transfer to ^{7}He unbound excited states [the ground state of ^{7}He cannot decay by the emission of an α particle, Fig. 1(a)]. Contributions arising from compound nucleus decay were estimated using statistical model calculations normalized to the measured fusion cross sections and are compared with the measured angular and energy distributions in Figs. 6(d) and 6(e). As can be seen from the Fig. 6(d), both the shape and amplitude of the angular distribution of ^{4}He particles, in coincidence with γ rays from ^{65,66}Cu at $E_{\rm lab} = 19.9$ MeV, are not consistent with those arising from a compound nuclear evaporation ($\alpha 2n$ and $\alpha 3n$) channels. Additionally, Fig. 6(e) shows that the energy distribution of ^{4}He particles is shifted

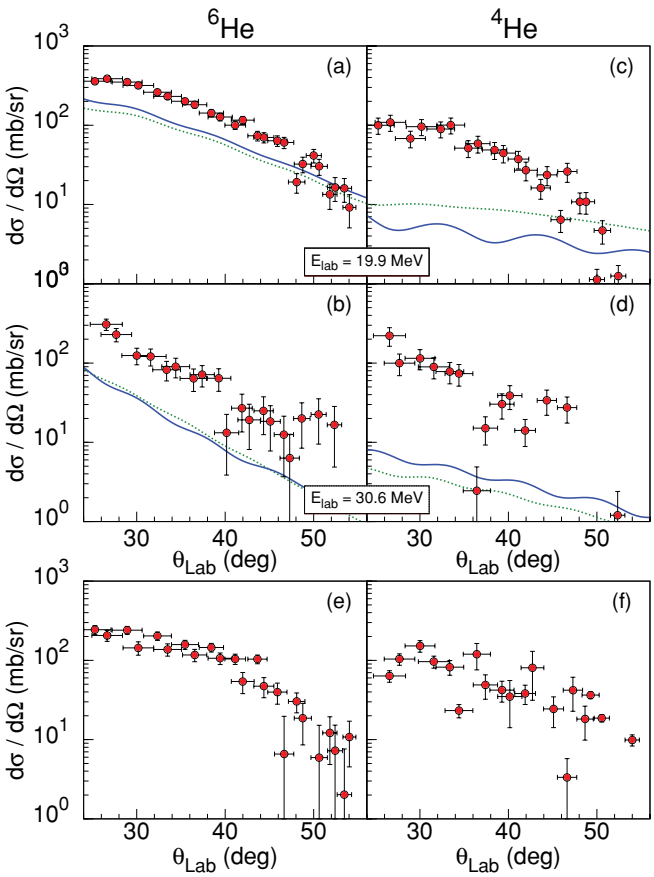

FIG. 7. (Color online) Neutron-transfer angular distributions obtained from the measurements of ^{4,6}He-γ coincidences: (a) ^{6}He angular distribution at $E_{\rm lab} = 19.9$ MeV in coincidence with either the 185.9-keV γ transition (^{66}Cu) or the 1115.5-keV γ transition (^{65}Cu). Standard (full lines) and *adjusted* (dotted lines) CRC calculations of neutron transfer to the ^{6,7}He(g.s.) are also shown (see Sec. III). (b) Same as (a) at $E_{\rm lab} = 30.6$ MeV (c) ^{4}He angular distribution at $E_{\rm lab} = 19.9$ MeV in coincidence with ^{65,66}Cu corrected for the compound nucleus contribution. Standard (full lines) and adjusted (dotted lines) CRC calculations of neutron transfer to the ^{6}He(2^{+}) are also shown (see Sec. III). (d) Same as (c) at $E_{\rm lab} = 30.6$ MeV. (e) Breakup angular distribution inferred from the difference between inclusive angular distribution of charged particles (^{4}He and ^{6}He) and total neutron transfer angular distribution at $E_{\rm lab} = 19.9$ MeV. The latter is shown in Fig. 8. (f) Same as (e) at $E_{\rm lab} = 30.6$ MeV. Only statistical errors are shown.

toward higher energies when compared with statistical model predictions. These two observations suggest that ^{4}He is also produced through a direct process, like transfer. Under the assumption that $3n$ and $4n$ transfers are negligible, ^{4}He-γ coincidences can be used to obtain information on the $1n$ and $2n$ transfers to ^{7}He and ^{6}He excited states. The corresponding angular distributions, obtained by subtracting the calculated compound nucleus contribution, are shown in Figs. 7(c) and 7(d). The total neutron-transfer angular distributions, obtained as the sum of the exclusive angular distributions of ^{6}He and ^{4}He, are shown in Fig. 8.

An attempt was also made to obtain angular distributions for the breakup of the projectile. Direct measurements of

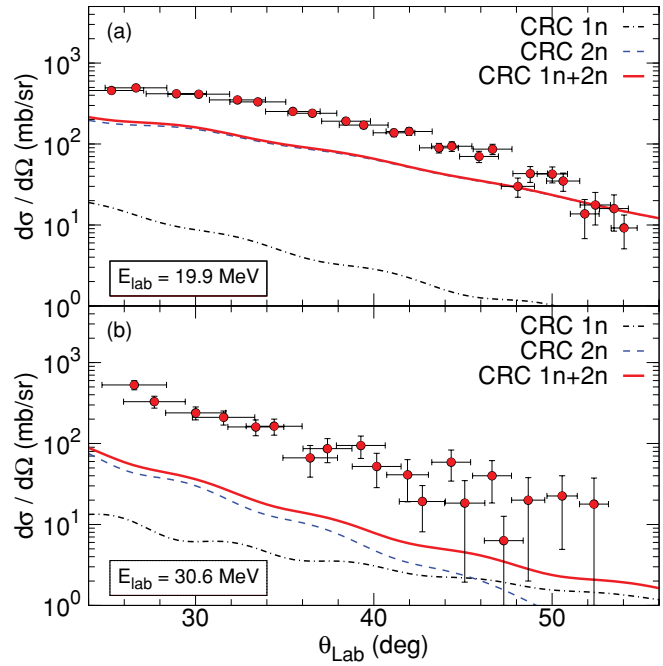

FIG. 8. (Color online) Total ($1n + 2n$) neutron-transfer angular distributions: (a) $1n + 2n$ transfer angular distribution at $E_{\rm lab} = 19.9$ MeV obtained from the sum of angular distributions of ^{6}He and ^{4}He in coincidence with γ transitions in ^{65,66}Cu shown in Figs. 7(a) and 7(c), respectively. Coupled reaction channels calculations (*standard*) for $1n + 2n$ transfer (full line), $1n$-transfer (dot-dashed line), and $2n$-transfer (dashed line) angular distributions are shown (see text for details). (b) Same as (a) at $E_{\rm lab} = 30.6$ MeV.

α-neutron correlations as used in Ref. [9] were not possible given the complexity of the structure of ^{8}He and the low beam intensity. Hence a different approach was used. Events from neutron transfer and breakup were separated using coincidences between γ rays emitted by the excited heavy targetlike transfer residues and light charged particles. The angular distribution for the breakup events was obtained from the difference between the inclusive and the total exclusive neutron-transfer cross sections (obtained from the ^{4,6}He-γ coincidences). Such an approach assumes that in a breakup processes ^{65}Cu is left in its ground state. The breakup angular distributions so obtained at $E_{\rm lab} = 19.9$ and 30.6 MeV, are shown in Figs. 7(e) and 7(f), respectively. It should be noted that these angular distributions represent an upper limit to the breakup process as they could contain contributions from a neutron-transfer process leading to the ground state of the targetlike residues where no γ rays are emitted.

In the case of the Borromean nucleus ^{8}He, the separation of the different ($1n/2n$) neutron-transfer channels on targets apart from hydrogen represents an experimental challenge. The final reaction products are similar for both $1n$ and $2n$ transfer so they cannot be directly differentiated from the measurement of either light or heavy targetlike products. Both the large Q value associated with the $2n$ transfer leading to neutron evaporation from the corresponding heavy residue and the unbound nature of ^{7}He prevent deconvolution of $1n$ and $2n$ transfer. In the case of ^{6}He [15], the construction of

the kinematic correlation between the energies and emission angles between ^{4}He particles and neutrons (that exists for $1n$ transfer but not for $2n$ transfer) in coincidence with γ rays from the excited heavy residue permitted the deconvolution of the the $1n$ and $2n$ transfer contributions. The nearly 200 times smaller beam intensity of ^{8}He prevented such an approach. Despite this, Fig. 6(b) shows a (triple) coincidence spectrum highlighting the sensitivity of the present work. This spectrum was obtained in coincidence with the full Neutron Wall array. The lower intensity of ^{8}He (compared to ^{6}He) prevented building the necessary kinematic correlation of energies and emission angles between ^{6}He (and also ^{4}He) particles and neutrons in coincidence with γ rays from the excited heavy residue. Additionally in the case of ^{8}He, as the ^{6,7}He excited states are unbound and decay to ^{4}He, this leads to a loss of kinematic correlations (Fig. 5). The separation of $1n$ and $2n$ transfer in the case of ^{8}He is beyond the scope of the present investigation. The first model-independent lower limits on the ratio of $2n$-to-$1n$ transfer cross sections involving ^{8}He are discussed elsewhere [41].

C. Elastic scattering

Elastic angular distributions of ^{8}He in the laboratory angular range between 25° and 60° at 19.9 and 30.6 MeV were obtained with inclusive measurements of ^{8}He and are shown in Fig. 9. Inelastic excitations to the 1115- and 1482-keV

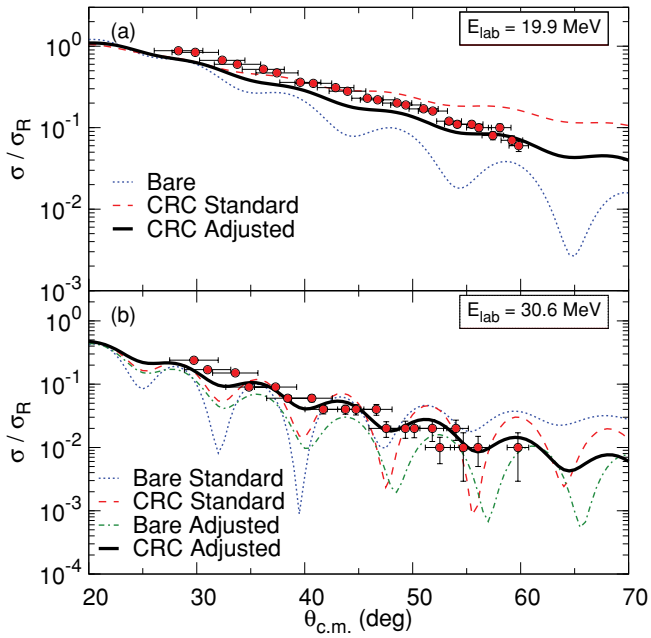

FIG. 9. (Color online) Elastic-scattering angular distributions: (a) at $E_{\rm lab} = 19.9$ MeV along no-coupling (bare) calculations (dotted line) and coupled reaction channels calculations including couplings to $1n$ and $2n$ transfer: *standard* (dashed line) and *adjusted* (full line) (see text). (b) At $E_{\rm lab} = 30.6$ MeV. Coupled reaction channels calculations (see text) with and without coupling for *standard* calculations: no coupling (dotted line) and with coupling (dashed line); and *adjusted* calculations: no coupling (dash-dotted line) and with coupling (full line). Only statistical errors are shown.

states of ^{65}Cu were studied using ^{8}He-γ coincidences. The corresponding differential cross sections were estimated to be ∼2 mb/sr in the measured angular range for both 19.9 and 30.6 MeV. This result is similar to those obtained in the $\alpha+^{65}$Cu system [57] and highlights the relatively small cross section of this process. In the next sections, these results for elastic scattering, neutron transfer, and fusion will be compared with coupled reaction channels calculations.

III. COUPLED REACTION CHANNELS CALCULATIONS

A simultaneous description of the measured elastic-scattering, neutron-transfer, and fusion cross sections was attempted using the CRC framework. The CRC calculations were performed using the code FRESCO [58]. Couplings of the elastic channel to the $1n$- and $2n$-transfer channels, ^{65}Cu(^{8}He,^{7}He(g.s.)) and ^{65}Cu(^{8}He,^{6}He(g.s.)) and ^{65}Cu(^{8}He,^{6}He(2^+)), were included. Coupling to breakup channels was not included, since ^{8}He is best described as a five-body object (four neutrons plus the α core), making it presently not possible to model realistically its complex breakup modes at these relatively low incident energies, unlike at much higher energies where eikonal methods may be applied, see, e.g., Ref. [59]. We therefore considered it better to omit this coupling altogether. Entrance and exit channel potentials consisted of double-folded real and interior Woods-Saxon imaginary parts. The Michigan three-range Yukawa (M3Y) effective interaction [60] and ^{8}He, ^{7}He, and ^{6}He matter densities from Refs. [61,62], and [63], respectively, were used to calculate the real potentials using the code DFPOT [64]. The ^{65,66,67}Cu densities were calculated using the liquid-drop model of Ref. [65]. The Woods-Saxon imaginary potential parameters were chosen to be: $W = 50$ MeV, $R = 1.0 \times (A_p^{1/3} + A_t^{1/3})$ fm, $a = 0.3$ fm. The interior imaginary potentials simulate the ingoing-wave boundary condition so in this model the total absorption cross section may be equated to the total fusion cross section. These calculations are similar to those discussed in Ref. [15] for the ^{6}He+^{65}Cu system. In the following, calculations employing interior imaginary potentials will be referred as "*standard calculations*." Calculations where the imaginary potential parameters in all partitions were adjusted to obtain better agreement with the elastic-scattering data will be referred to as "*adjusted calculations*."

The positive Q value (+4.48 MeV) of the ^{65}Cu(^{8}He,^{7}He)^{66}Cu reaction favors population of relatively high-lying states. However, the $(2J+1)S$ values derived from an analysis of the ^{65}Cu(d,p) reaction show a rather rapid decrease with increasing excitation energy (below 3 MeV) [54]. Thus, a limited number of states in ^{66}Cu were included. Inclusion of the $2n$-transfer channel in the calculations is more challenging, as the Q value for this reaction (+14.04 MeV) favors high-lying states in ^{67}Cu in an excitation energy region where no structure information is available. The Q-matching condition, together with the fact of the nonobservation of ^{67}Cu, suggests that, if the mechanism is conventional transfer, only states above the $1n$ separation threshold in ^{67}Cu (9.1 MeV) should be considered. Because of the lack of information on high-lying states in ^{67}Cu we

extrapolated the similarity of the low-lying spectra of ^{65}Cu and ^{67} Cu observed in (p, t) reactions [66] to higher excitation energies. All known states (above 10.9 MeV) in ^{65}Cu [67] were included. A dineutron-like cluster structure for these states with the lowest possible $2n$ angular momentum relative to the ^{65}Cu ground state was assumed. Coupling between the ^{6}He 0^+ ground and 2^+ excited states in the ^{65}Cu(^{8}He,^{6}He)^{67}Cu $2n$-transfer exit channel was also included, with $B(E2)$ and δ_2 values from Ref. [31], but two-step sequential transfer was omitted due to lack of knowledge of the specific structure of the targetlike states involved. Although the sequential transfer could be more important here than in the ^{6}He+^{65}Cu system, particularly for the population of the ^{6}He (2^+) state [31], we chose to omit it rather than introduce possibly spurious effects into the calculations [15]. In any case, extrapolation of the importance of two-step transfer paths from the (p,t) analysis to the present system is problematic, given the very different kinematic conditions [31]. The n+^{65}Cu and $2n$+^{65}Cu form factors and spectroscopic factors were as in Ref. [15], while those for n+^{7}He and $2n$+^{6}He were taken from Ref. [31]. The full complex remnant terms and nonorthogonality corrections were included.

IV. RESULTS AND DISCUSSION

The *standard* CRC calculations (dashed lines) are compared in Fig. 9 with the elastic-scattering angular distributions and the "bare" no-coupling calculations (dotted lines) that do not include couplings to transfer channels. The significant effect of the couplings can be seen from the figure at both energies, being larger at 19.9 MeV. This observation is consistent with the known energy dependence of coupling effects that tend to reduce in importance as the incident energy is increased above the Coulomb barrier. However, in neither case can the full CRC calculations be said to reproduce well the data. In particular, at 19.9 MeV, it is clear that the slope of the CRC calculation (dashed line) is much less steep than the data, suggesting that the coupling effect is too large. This problem will be discussed below, in the light of the second set of calculations (*adjusted*).

In Figs. 7(a) and 7(b), the standard calculations for the sum of $1n + 2n$ transfer to the ground states of ^{7}He and ^{6}He, respectively (full lines), are compared with the measured cross sections. As the reaction mechanism(s) are not separated experimentally it is not possible to transform them to the center-of-mass reference frame, hence the measured cross sections are presented in the laboratory frame, as are the calculations. Note that the calculated angular distributions for population of the ^{7}He ground state by $1n$ transfer are presented as a function of the ^{7}He laboratory angle, whereas the data are a function of the detected ^{6}He laboratory angle (as the unbound ^{7}He decays exclusively into ^{6}He(g.s.) + n). However, the difference between the two angles is negligible. While the shapes of the angular distributions are well reproduced by the calculations, their magnitudes are not. At 19.9 MeV [Fig. 7(a)] the calculations are a factor of $\sim$2 smaller than the data while at 30.6 MeV [Fig. 7(b)] they are $\sim$5 times smaller. The good reproduction of the shape of the angular distributions at both energies suggests that the basic production mechanism is direct $1n$ and $2n$ transfer, as modeled in the calculations. The discrepancy in magnitude could be explained by the necessarily conjectural nature of the ^{67}Cu = $2n$+^{65}Cu form factors. The excitation energies and spin parities of known states in ^{65}Cu were taken as a basis for the ^{65}Cu:^{67}Cu overlaps, setting the spectroscopic amplitudes equal to 1.0. As the present data also include coincidences with the 1115.5-keV γ transition in ^{65}Cu, transfer to states above the $2n$ emission threshold in ^{67}Cu may account for the greater part of the difference between measured and calculated cross sections, as such states were not included in the calculations due to lack of available spectroscopic information. More complicated reaction mechanisms such as the ^{65}Cu(^{8}He,^{7}He)^{66}Cu(^{7}He,^{6}He)^{67}Cu two-step transfer could also contribute to the "missing" cross section. However, the worse quantitative agreement with the measured cross section at the higher incident energy suggests that a significant portion of the reaction mechanism is missing from the calculations. As the incident energy increases more reaction channels open as the increased available energy provides access to higher-lying states in both projectile-like and targetlike nuclei. The importance of multistep transfer paths will also vary with energy. The increased available energy at 30.6 MeV might favor these processes but would also give access to more higher-lying states in ^{67}Cu for direct $2n$ stripping. Thus, the increased quantitative difference between calculated and measured cross sections at 30.6 MeV is consistent with either or both of these explanations for the missing cross section.

In Figs. 7(c) and 7(d), the calculated angular distributions for populating the unbound ^{6}He 2^+_1 state via $2n$ stripping (full lines) are compared with the measurements. The measured angular distributions are presented in the laboratory frame and the calculated ^{65}Cu(^{8}He,^{6}He(2^+_1))^{67}Cu cross sections have been transformed accordingly. The calculated cross sections are therefore a function of the ^{6}He(2^+_1) laboratory angle rather than that of the detected ^{4}He; while the difference between these two quantities will be larger than for the ^{7}He case it should not significantly affect the conclusions. The calculated angular distributions underpredict the magnitude of the data (by about a factor of 10 at the most forward angles measured) and also fail to describe the shape. This cannot be ascribed to the slight differences between the laboratory angles of the calculated ^{6}He(2^+_1) and the measured ^{4}He cross sections and suggests that the main production mechanism for α particles is some other reaction process. The most likely candidates contributing to the α particles are $1n$ stripping to higher-lying states in ^{7}He and $2n$ stripping to higher-lying states in ^{6}He (in both cases the projectile-like residue could decay to give α particles).

The calculated $1n + 2n$ transfer angular distributions (full lines) are compared with the sum of ^{6}He and ^{4}He exclusive angular distributions in Figs. 8(a) and 8(b). Also shown in the figure are the individual calculated contributions for $1n$ (dot-dashed lines) and $2n$ (dashed lines). The calculated $1n$-stripping cross sections are almost an order of magnitude smaller than the $2n$ stripping. The ^{8}He:^{7}He and ^{65}Cu:^{66}Cu spectroscopic amplitudes are well known, and the calculations are expected to be realistic for the $1n$ channel. This is suggested by the rather good agreement between similar calculations and the measured $1n$-stripping cross sections in the ^{6}He+^{65}Cu

system [15], confirming that at least the ^{65}Cu:^{66}Cu overlap is reasonably accurate in description.

Finally, the fusion and total integrated transfer cross sections are compared with the predictions of CRC calculations in Fig. 4(b). The amplitudes of the fusion cross sections are in reasonable agreement at both energies. The integral neutron-transfer cross sections are underpredicted, which is consistent with the similar behavior of the differential cross sections.

The tendency of the set of *standard* calculations with interior imaginary potentials in all partitions to overestimate the coupling effect on the elastic-scattering angular distribution was mentioned earlier. This is a more or less general problem with this type of calculation: the lack of surface absorption in the exit partition optical potentials (here the ^{7}He+^{66}Cu and ^{6}He+^{67}Cu potentials) tends to lead to an overprediction of both the transfer cross section itself and its coupling effect on the elastic scattering. Ideally, one would like to alleviate this problem by adding the strongest inelastic couplings between channels in the exit partitions, for example, but in this case, where the projectile-like nuclei are either weakly bound or unbound and a large number of states in the targetlike residues are populated, this is not possible. The effect of such couplings may be simulated to some extent by increasing the radius and diffuseness parameters of the imaginary parts of the optical potentials in the exit partitions, at the cost of no longer being able to equate the total absorption cross section with the total fusion cross section. Therefore, in order to test the robustness of the conclusions, a second set of calculations (referred to as "adjusted"), where the imaginary potentials in all partitions were allowed to vary to obtain the best agreement with the elastic scattering, was performed. The normalizations of the double-folded real potentials were not varied in order to reduce the number of adjustable parameters. Although the elastic scattering is sensitive to the strength of the real potential, this is mainly in the region of Coulomb-nuclear interference where no data are available, making a realistic adjustment of this parameter impossible in this case. The final "best fit" imaginary potential parameters at both energies are given in Table I.

The *adjusted* calculations (thick full lines) are compared with the elastic-scattering data in Figs. 9(a) and 9(b). A significant coupling effect on the elastic scattering can be seen at both energies, being more pronounced at 19.9 MeV.

TABLE I. Imaginary potential parameters for the adjusted calculations at 19.9 and 30.6 MeV. The potentials are of volume Woods-Saxon form and use the radius convention: $R_W = r_W \times (A_p{}^{1/3} + A_t{}^{1/3})$ fm.

E (MeV)	Partition	W (MeV)	r_W (fm)	a_W (fm)
19.9	^{65}Cu(^{8}He, ^{8}He)^{65}Cu	50.0	1.00	0.30
	^{65}Cu(^{8}He, ^{7}He)^{66}Cu	50.0	1.45	0.60
	^{65}Cu(^{8}He, ^{6}He)^{67}Cu	50.0	1.45	0.60
30.6	^{65}Cu(^{8}He, ^{8}He)^{65}Cu	20.0	1.30	0.40
	^{65}Cu(^{8}He, ^{7}He)^{66}Cu	50.0	1.30	0.60
	^{65}Cu(^{8}He, ^{6}He)^{67}Cu	50.0	1.30	0.60

While the overall coupling effect is now rather smaller than it was for the standard calculations [see Figs. 9(a) and 9(b)] the shape of the angular distributions is better reproduced. Then, in Figs. 7(a) and 7(b), the corresponding calculations (dotted lines) are compared with the exclusive ^{6}He angular distributions and the *standard* calculations (full lines). Over the measured angular range, the calculated cross sections do not differ significantly from those of the standard calculations. The increased surface strength of the imaginary potentials in the exit partitions compared to the standard calculations also damps out the oscillations in the calculated angular distributions. As can be seen from Figs. 7(c) and 7(d), similar observations also hold for the α-particle cross sections. The shape of the calculated angular distributions is not significantly affected, tending to confirm the supposition that other reaction paths than direct $2n$ stripping to the ^{6}He 2_1^+ state make the largest contribution to the α-particle production cross section.

To summarize, both sets of calculations, standard and adjusted, are in reasonable qualitative agreement with the data. Given the uncertainties in the $2n$-stripping part of the calculations and the apparent dominance of this reaction in the production of ^{6}He, qualitative agreement is all that can reasonably be achieved. Nevertheless, the level of agreement does enable us to draw some general conclusions. It should be noted that the incident energies considered here, 19.9 and 30.6 MeV, are considerably larger than the nominal Coulomb barrier for the ^{8}He+^{65}Cu system (7.63 MeV when defined as the maximum of the combined double-folded nuclear and Coulomb potentials). Therefore, the coupling effects and, to a lesser extent, the transfer cross sections are expected to be relatively less important than they would be at lower incident energies. Conventional $1n$- and $2n$-stripping reactions to *bound* states of the targetlike residual nuclei generate a significant, even large, coupling effect at these relatively high incident energies compared to the nominal Coulomb barrier. The higher-lying states populated in ^{67}Cu may subsequently decay by the emission of a single-neutron rather than a γ ray, but this does not affect the fact that the reaction mechanism is conventional transfer rather than "transfer to the continuum," which may be formally equated with breakup. The significant coupling effect is robust in that it does not depend on the choice of imaginary potentials except in detail; the adjusted calculations show a smaller (but still important) coupling effect on the elastic scattering, which is probably the more realistic of the two. This large coupling effect due to neutron stripping seems to be more or less unique to the neutron-rich exotic nuclei, see, e.g., Ref. [2], although a low neutron separation energy is a necessary rather than a sufficient condition, as the spectroscopic factors also play an important role.

The present exclusive measurements of neutron transfer using particle-γ coincidences indicate that these cross sections are large for the interaction of ^{8}He with ^{65}Cu. Large integral transfer cross sections, even larger than the fusion cross sections at energies around the Coulomb barrier, were earlier reported in the ^{8}He+^{197}Au system [22]. The simultaneous measurement of elastic-scattering and neutron-transfer angular distributions and the comparison with coupled reaction channels calculations highlights the significant effect of the coupling to the transfer channels on the elastic channel. Recently,

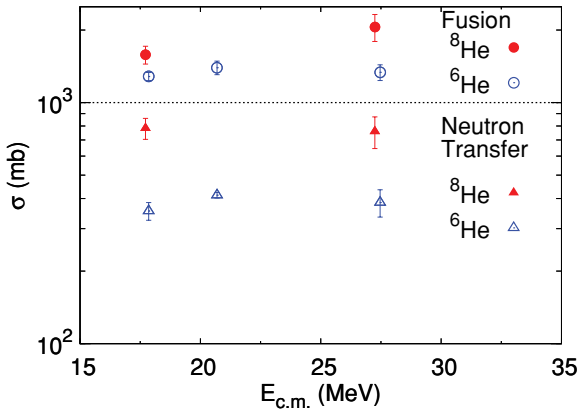

FIG. 10. (Color online) Fusion and transfer excitation functions for the systems ^{6,8}He+^{65}Cu. The ^{6}He data are taken from Refs. [14,15].

measurements of elastic scattering in the ^{9,10,11}Be + ^{64}Zn system at an energy above the barrier have been reported. This work used an optical model approach to point out the difference between ^{11}Be and other isotopes. The observed differences were attributed to arise either from the role of transfer or the breakup channel [68]. The relative importance of the 2n transfer channel in the ^{6}He+^{208}Pb system was also highlighted in Ref. [69]. Figure 10 shows a comparison of the measured fusion and transfer cross sections for the Borromean nuclei ^{6,8}He on a ^{65}Cu target. At these relatively high energies with respect to the barrier, where the elastic scattering is on the edge of the Fraunhofer scattering regime, the total transfer cross section is still comparable (around a factor of 2 lower) to the fusion cross section. This differs significantly from the behavior for reactions involving "normal" nuclei. The effect is even more pronounced in the case of ^{8}He, where the extra neutrons do not significantly increase the fusion cross section but contribute to the increased transfer cross sections [22].

V. SUMMARY AND CONCLUSION

In summary, this work presents the first and most complete study of direct reactions induced by ^{8}He that could be performed with currently available beam intensities at energies around the Coulomb barrier. Results for fusion, elastic scattering, neutron transfer, and breakup of ^{8}He on ^{65}Cu have been presented. Inclusive measurements of γ rays and charged particles were used to obtain respectively fusion and neutron-transfer cross sections and elastic-scattering angular distributions. Exclusive coincidence measurements involving charged particles and γ rays were used to obtain neutron-transfer angular distributions. Breakup angular distributions were inferred from these exclusive measurements. Large neutron-transfer cross sections were obtained. Coupled reaction channels calculations were used to illustrate the important role played by the transfer channel in understanding reactions involving weakly bound Borromean nuclei.

The most surprising result is the relatively very large total ($1n + 2n$) transfer cross section with respect to the fusion cross section, see Fig. 10. At these relatively large incident energies, almost into the Fraunhofer scattering regime, direct reaction cross section are usually much smaller than those for fusion, yet here the total transfer cross sections are only about a factor of 2 smaller than the measured fusion cross sections. A suitable comparison with stable nuclei is not obvious, but perhaps the nearest stable analog to the radioactive ^{8}He nucleus is ^{9}Be. Of course, the parallel is not complete, as ^{9}Be only has a large 1n-transfer probability. However, Figure 20 of Ref. [2] shows that for somewhat lower energies—still well within the Fresnel scattering regime—the 1n-transfer cross section for the ^{9}Be + ^{208}Pb system is already over an order of magnitude smaller than the fusion cross section at energies a few MeV above the Coulomb barrier. Thus, the present data underline previous conclusions concerning the influence of the specific structure of ^{8}He on its reaction mechanisms: The extra valence neutrons lead to a dominance of transfer reactions, and this dominance continues up to much larger energies than would be inferred by extrapolating studies with stable nuclei. A similar situation holds for ^{6}He (see Fig. 10) but with relatively smaller transfer cross sections compared to ^{8}He, strongly suggesting that the effect of correlations among the valence neutrons is such that transfer of these nucleons is favored over other reactions, including to some extent the projectile breakup.

The feasibility of measuring absolute cross sections using *inclusive* in-beam γ-ray measurements with 10^5 pps ISOL radioactive beams has been demonstrated. Such measurements have been made possible owing to very good beam quality in conjunction with highly efficient detector systems and open new possibilities for in-beam reaction studies with low-intensity RIB at present and future facilities.

The significant cross sections for neutron transfers with RIB at energies near the Coulomb barrier make it a possible probe to investigate the structure of these weakly bound nuclei. For example, the relative cross sections for 1n and 2n transfer could provide an insight into the spatial correlations of the valence neutrons in Borromean nuclei and pairing properties. However, the "double-Borromean" structure of ^{8}He and the present beam intensities prevent the individual determination of 1n and 2n transfer cross sections using the kinematic correlations suggested in Ref. [15]. Alternative experimental approaches like that discussed in Ref. [41] will be required to explore new reactions involving Borromean nuclei in more detail.

ACKNOWLEDGMENTS

We acknowledge the GANIL staff for obtaining the highest quality of re-accelerated ^{8}He beams and for all technical aspects. We especially thank J. Ropert, G. Volotoni, G. Fremont, and C. Spitaels for their technical contributions. The authors also thank V. Zelevinsky for insightful discussions and W. Mittig for useful suggestions during the experiment. The European Gamma-ray Spectroscopy Pool is thanked for permitting the Neutron Wall to be installed at GANIL. This work was supported in part by the Polish Ministry of Science and Higher Education (Grant No. N202 033637) and the Swedish Research Council. A.L. was partly supported by the Région Basse-Normandie (France).

[1] L. Canto, P. Gomes, R. Donangelo, and M. Hussein, Phys. Rep. **424**, 1 (2006).
[2] N. Keeley, N. Alamanos, K. Kemper, and K. Rusek, Prog. Part. Nucl. Phys. **63**, 396 (2009).
[3] A. Navin, F. De Oliveira, P. Roussel-Chomaz, and O. Sorlin, J. Phys. G (to be published).
[4] N. Keeley, R. Raabe, N. Alamanos, and J. Sida, Prog. Part. Nucl. Phys. **59**, 579 (2007).
[5] M. V. Zhukov, B. V. Danilin, D. V. Fedorov, J. M. Bang, I. J. Thompson, and J. S. Vaagen, Phys. Rep. **231**, 151 (1993).
[6] K. Tanaka *et al.*, Phys. Rev. Lett. **104**, 062701 (2010).
[7] I. Thompson and F. Nunes, *Nuclear Reactions for Astrophysics* (Cambridge University Press, Cambridge, 2009).
[8] K. Hagino, A. Vitturi, C. H. Dasso, and S. M. Lenzi, Phys. Rev. C **61**, 037602 (2000).
[9] J. J. Kolata *et al.*, Phys. Rev. C **75**, 031302(R) (2007).
[10] L. R. Gasques, D. J. Hinde, M. Dasgupta, A. Mukherjee, and R. G. Thomas, Phys. Rev. C **79**, 034605 (2009).
[11] E. F. Aguilera *et al.*, Phys. Rev. C **80**, 044605 (2009).
[12] L. F. Canto, P. R. S. Gomes, J. Lubian, L. C. Chamon, and E. Crema, J. Phys. G **36**, 015109 (2009).
[13] V. Tripathi, A. Navin, K. Mahata, K. Ramachandran, A. Chatterjee, and S. Kailas, Phys. Rev. Lett. **88**, 172701 (2002).
[14] A. Navin *et al.*, Phys. Rev. C **70**, 044601 (2004).
[15] A. Chatterjee *et al.*, Phys. Rev. Lett. **101**, 032701 (2008).
[16] A. Di Pietro *et al.*, Phys. Rev. C **69**, 044613 (2004).
[17] Y. Penionzhkevich *et al.*, Eur. Phys. J. A **31**, 185 (2007).
[18] J. P. Bychowski *et al.*, Phys. Lett. B **596**, 26 (2004).
[19] P. A. DeYoung *et al.*, Phys. Rev. C **71**, 051601 (2005).
[20] R. Raabe *et al.*, Nature **431**, 823 (2002).
[21] R. Raabe, C. Angulo, J. L. Charvet, C. Jouanne, L. Nalpas, P. Figuera, D. Pierroutsakou, M. Romoli, and J. L. Sida, Phys. Rev. C **74**, 044606 (2006).
[22] A. Lemasson *et al.*, Phys. Rev. Lett. **103**, 232701 (2009).
[23] D. R. Tilley, C. M. Cheves, J. L. Godwin, G. M. Hale, H. M. Hofmann, J. H. Kelley, C. G. Sheu, and H. R. Weller, Nucl. Phys. A **708**, 3 (2002).
[24] D. Tilley, J. Kelley, J. Godwin, D. Millener, J. Purcell, C. Sheu, and H. Weller, Nucl. Phys. A **745**, 155 (2004).
[25] A. H. Wuosmaa *et al.*, Phys. Rev. C **78**, 041302 (2008).
[26] X. Mougeot, Ph.D. thesis, Université Paris Diderot, 2008.
[27] W. N. Catford *et al.*, Nucl. Instrum. Methods **371**, 449 (1996).
[28] P. Mueller *et al.*, Phys. Rev. Lett. **99**, 252501 (2007).
[29] V. L. Ryjkov *et al.*, Phys. Rev. Lett. **101**, 012501 (2008).
[30] F. Skaza *et al.*, Phys. Rev. C **73**, 044301 (2006).
[31] N. Keeley *et al.*, Phys. Lett. B **646**, 222 (2007).
[32] L. Chulkov *et al.*, Nucl. Phys. A **759**, 43 (2005).
[33] K. Markenroth *et al.*, Nucl. Phys. A **679**, 462 (2001).
[34] M. Meister *et al.*, Nucl. Phys. A **700**, 3 (2002).
[35] M. Golovkov *et al.*, Phys. Lett. B **672**, 22 (2009).
[36] M. V. Zhukov, A. A. Korsheninnikov, and M. H. Smedberg, Phys. Rev. C **50**, R1 (1994).
[37] K. Hagino, N. Takahashi, and H. Sagawa, Phys. Rev. C **77**, 054317 (2008).
[38] A. A. Korsheninnikov *et al.*, Phys. Rev. Lett. **90**, 082501 (2003).
[39] Y. Kanada-En'yo, Phys. Rev. C **76**, 044323 (2007).
[40] G. Potel *et al.*, arXiv:0906.4298.
[41] A. Lemasson *et al.* (submitted).
[42] A. C. C. Villari, Nucl. Phys. A **693**, 465 (2001).
[43] J. Simpson *et al.* (EXOGAM Collaboration), Acta Phys. Hung. New Ser.: Heavy Ion Phys. **11**, 159 (2000).
[44] O. Skeppstedt *et al.*, Nucl. Instrum. Methods A **421**, 531 (1999).
[45] Z. Podolyák *et al.*, Nucl. Instrum. Methods A **511**, 354 (2003).
[46] P. Gomes, T. Penna, R. L. Neto, J. Acquadro, C. Tenreiro, P. Freitas, E. Crema, N. C. Filho, and M. Coimbra, Nucl. Instrum. Methods A **280**, 395 (1989).
[47] F. Pühlhofer, Nucl. Phys. A **280**, 267 (1977).
[48] A. V. Ignatyuk, G. N. Smirenkin, and A. S. Tishin, Sov. J. Nucl. Phys. **21**, 255 (1975).
[49] D. Wilmore and P. E. Hodgson, Nucl. Phys. **55**, 673 (1964).
[50] F. D. Becchetti and G. W. Greenlees, Phys. Rev. **182**, 1190 (1969).
[51] L. McFadden and G. R. Satchler, Nucl. Phys. **84**, 177 (1966).
[52] C. H. Dasso and S. Landowne, Comput. Phys. Commun. **46**, 187 (1987).
[53] Ö. Akyüz and A. Winther, *Proceedings of the Enrico Fermi International School of Physics 1979* (North-Holland, Amsterdam, 1981).
[54] W. W. Daehnick and Y. S. Park, Phys. Rev. **180**, 1062 (1969).
[55] G. R. Satchler, *Direct Nuclear Reactions* (Oxford University Press, Oxford, 1983).
[56] D. Brink, Phys. Lett. B **40**, 37 (1972).
[57] M. Ivascu, G. Semenescu, D. Bucurescu, and M. Titirici, Nucl. Phys. A **147**, 107 (1970).
[58] I. J. Thompson, Comput. Phys. Rep. **7**, 167 (1988).
[59] J. Tostevin, J. S. Al-Khalili, M. Zahar, M. Belbot, J. J. Kolata, K. Lamkin, D. J. Morrissey, B. M. Sherrill, M. Lewitowicz, and A. H. Wuosmaa, Phys. Rev. C **56**, R2929 (1997).
[60] G. R. Satchler and W. G. Love, Phys. Rep. **55**, 183 (1979).
[61] P. Navrátil and B. R. Barrett, Phys. Rev. C **57**, 3119 (1998).
[62] T. Neff and H. Feldmeier, Nucl. Phys. A **738**, 357 (2004).
[63] J. S. Al-Khalili, J. A. Tostevin, and I. J. Thompson, Phys. Rev. C **54**, 1843 (1996).
[64] J. Cook, Comput. Phys. Commun. **25**, 125 (1982).
[65] W. D. Myers, Nucl. Phys. A **145**, 387 (1970).
[66] J. H. Bjerregaard, O. Nathan, S. Hinds, and R. Middleton, Nucl. Phys. **85**, 593 (1966).
[67] M. R. Bhat, Nucl. Data Sheets **83**, 789 (1998).
[68] A. Di Pietro *et al.*, Phys. Rev. Lett. **105**, 022701 (2010).
[69] J. P. Fernández-García, M. A. G. Alvarez, A. M. Moro, and M. Rodríguez-Gallardo, Phys. Lett. B **693**, 310 (2010).